Ryerson University
Department of Electrical, Computer & Biomedical Engineering
Faculty of Engineering & Architectural Science

DX05: V2G ELECTRICAL VEHICLE QUICK CHARGER

by
Raghuvinder Riat, Nicholas Leong, Brian Zhen, Ayotomiwa Borisade

Electrical Engineering Capstone Design Project
Ryerson University, 2022

Acknowledgements

First, we have to thank our research supervisor, Dr. David Xu for their assistance throughout the project. We would also like to thank Dr. Sandeep Kaler for his help at the beginning of the project.

Most importantly, none of this could have happened without our families. To our parents and grandparents – it would be an understatement to say that, as a family, we have experienced some ups and downs in the past year. This report stands as a testament to your unconditional love and encouragement.

Certification of Authorship

We hereby certify that we are the authors of this document and that any assistance we received in its preparation is fully acknowledged and disclosed in the document. We have also cited all sources from which we obtained data, ideas, or words that are copied directly or paraphrased in the document.

Raghuvinder Riat
Nicholas Leong
Brian Zhen
Ayotomiwa Borisade

Table of Contents

Abstract

The design objective of this project is to design and simulate a two-stage electric vehicle quick charger with bidirectional power flow. The simulation is to be performed using MATLAB Simulink. The converter is required to connect to the grid and supply full power to the battery at 60kW. The three-phase grid side voltage is required to be 420V AC at 60Hz. It is required to have a 340V nominal output with a charging capability of up to 150A and a voltage charging range of 200V to 420V. The grid side current THD is required to be less than 5%. There must be galvanic isolation between the grid and the battery.

The project was carried out by designing and testing the two stages separately with the goal of combining them once each stage was completed. Each stage was simulated using MATLAB Simulink under the required conditions. A three phase grid was used to represent the grid and a lithium-ion battery was used to represent the EV battery. The battery had a nominal nominal voltage of 340V with a total capacity of 150Ah for the sake of testing the charging requirements.

The ACDC converter was able to meet the requirements of bidirectional power flow, grid interface, and current THD of less than 5% but was not able to meet the rated power requirement due to the selection of the filter inductance. The DAB was able to meet the requirement of constant voltage charging but was not able to meet the requirement of constant current charging. Due to unsuccessful completion of each stage, the two stages could not be combined and tested as a two-stage converter as required.

Introduction & Background

Canada is projected to sell only ZEVs by 2035 and it's important to be able to benefit from this movement. With a 500 million dollar investment by the Canada Infrastructure Bank and 400 million dollars for the Zero Emission Vehicle Infrastructure Program, the goal for Canada is to add 50,000 charging stations throughout the country. As of March 31, 2022, Canadians have purchased or leased over 141,000 new ZEVs, thanks to the Zero-Emission Vehicles Program. With the increase in ZEVs, demand for chargers also increase. Projects that will develop more than 25,000 charging stations have since been approved by the Government of Canada.[7] The increased use of electric vehicles also presents the opportunity to use the electric vehicle batteries to contribute stored energy to the grid to realize the function of vehicle to grid (V2G). Assisting the grid whenever needed, the batteries lessen the stress on the grid. Other benefits include a reduction in grid congestion and it is predicted that in the future, consumers that enable their car batteries to be used as balancing elements can be rewarded.

A single system with bidirectional flow of power can be used to realize both functions of battery charging and V2G. The purpose of this project is to develop an electric vehicle battery quick charger that can also function as a grid connected power source. This will be done by using a two-stage power converter with bidirectional power flow. First stage being an AC-DC converter with a three-phase input and an accompanying controller and the later stage being a Dual Active Bridge converter with a controller to meet the various charging requirements.

Objectives

The objective of this project is to design and simulate an electric vehicle quick charger with bidirectional power flow. The simulation is to be performed using MATLAB Simulink.

- The converter is required to connect to the grid and supply full power to the battery at 60kW.
- The three-phase grid side voltage is required to be 420V AC at 60Hz.
- It is required to have a 340V nominal output with a charging capability of up to 150A and a voltage charging range of 200V to 420V.
- The grid side current THD is required to be less than 5% to minimize power losses and harmonic distortion in the current contributed to the grid.
- There must be galvanic isolation between the grid and the battery, which is provided by the high-frequency transformer in the dual-active-bridge.

Theory and Design

This chapter outlines the theories behind our methods and models, while providing detailed explanations for such choices. The explanation of all blocks are included, with a description of how each functions. The source of parameters are also discussed in this section. This chapter also covers the importance of each block and how it contributes to our final design. Included are steps and design decisions made to fulfill requirements outlined under Objectives. First, the discussion of the AC-DC converter, then its controller. After that, the DC-DC converter and its controller will be discussed.

1. Block diagram

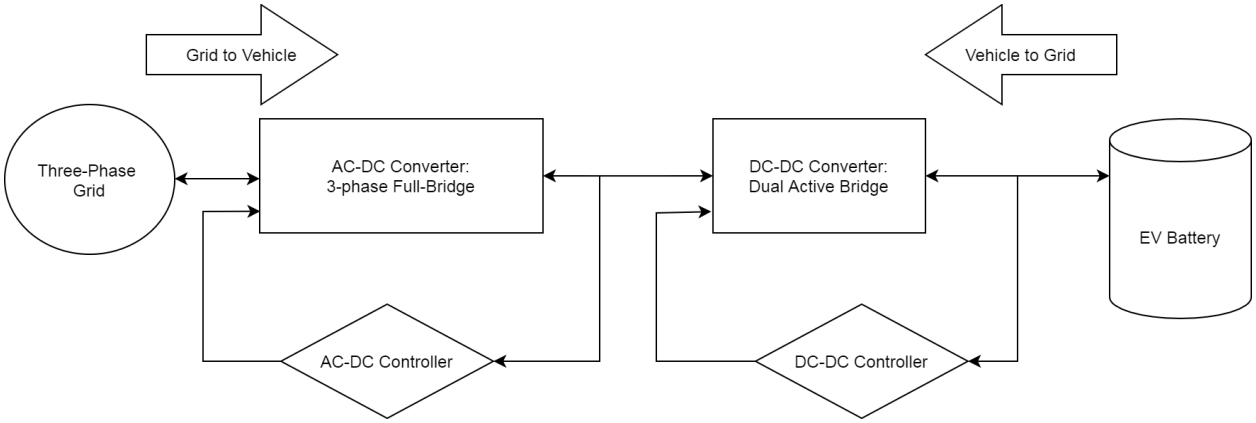

Figure 1.1: Block diagram of the proposed system

The above diagram shows the overview of the two stage converter. The ACDC converter connects to the grid through an inductance filter on one side and the Dual Active Bridge(DAB) on the other side. The DAB connects to the EV battery. Both converters have controllers to ensure their respective outputs are controlled based on certain requirements. A detailed explanation of each converter and their controller is given below.

2-1. AC-DC Converter

The AC-DC converter is responsible for drawing power from the grid and converting it to DC form for use by the DC-DC converter and the battery in rectifier mode. In rectifier mode, the converter is to draw 420V RMS from the grid at 60hz and convert it to 567V DC. In inverter mode the AC-DC converter converts the DC voltage drawn from the battery to an AC voltage matching the grid voltage and frequency. The current contributed to the grid is required to have a THD of less than 5%. The following closed loop control scheme will be used to achieve bidirectional control of the converter.

Full bridge Converter Block Diagram

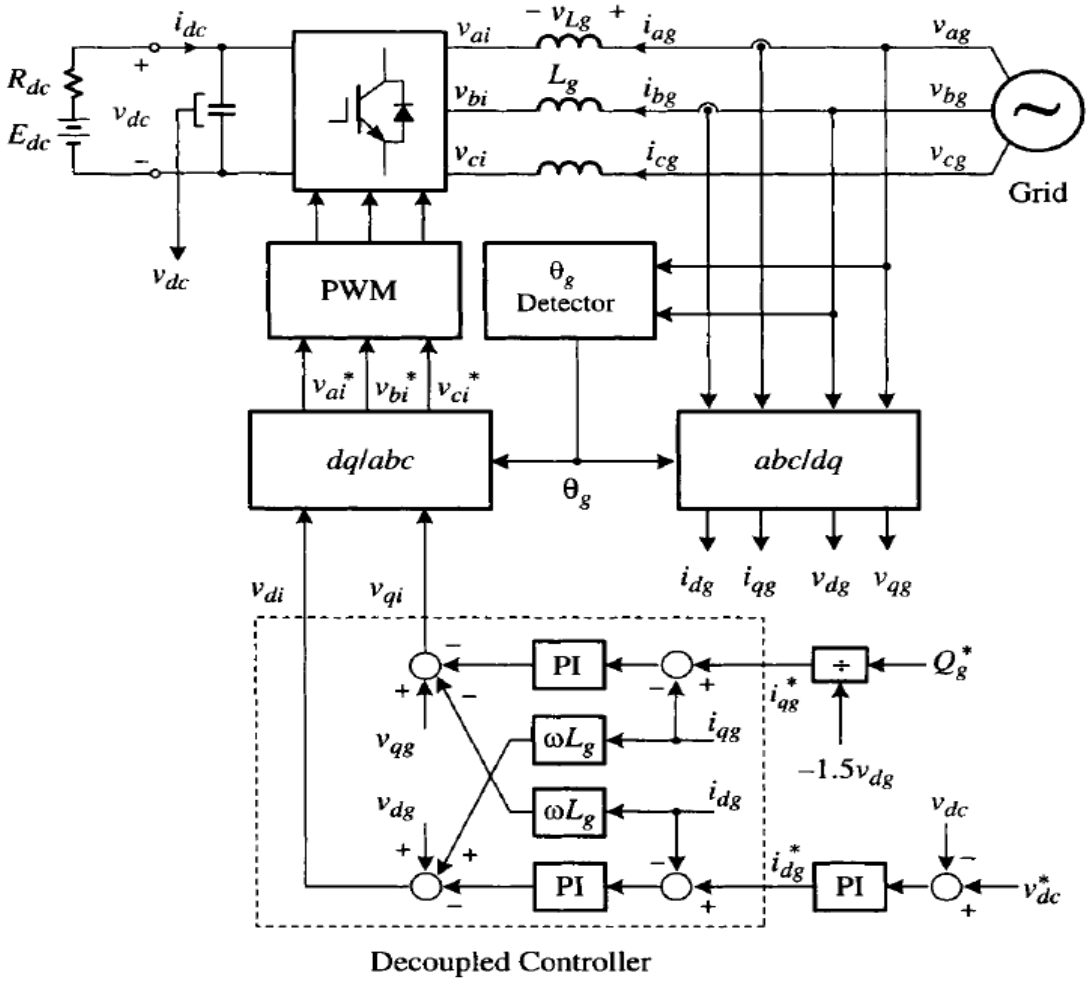

Figure 2.1: The three phase converter and its closed loop control scheme [1]

A detailed description of each block of the controller is given in the following sections. The control scheme used per unit values of the quantities in order to simplify control. The base values used for the per-unit system are given below:

Base Apparent Power = Rated Grid power / 3
Base frequency = 60Hz
Base Electrical Frequency = 2*pi*60
Base Voltage = Grid side line to line voltage $/\sqrt{3}$
Base Current = Base Power / Base Voltage
Base Impedance = Base Voltage / Base Current
Base Inducance = Base Impedance / Base Electrical Frequency
Base Capacitance = 1/ (Base impedance * Base Electrical Frequency)

Various filters were used at different stages of the controller in order to minimize the noise of the incoming signals before they input into the PI controllers. The cutoff frequency of these controllers was set at 5% to 10% of the switching frequency.

2-2. Block Diagram Descriptions

Three Phase IGBT Bridge

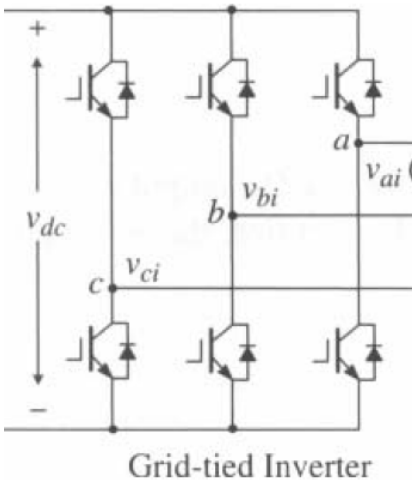

Figure 2.2: Circuit diagram of the three phase IGBT full bridge converter[1]

Figure 2 shows the schematic diagram of the full bridge converter. It is composed of three half bridge legs - one for each phase of the AC side voltage - each consisting of two IGBT switches. IGBTs are used since they are better suited for high-current applications. The DC side of the converter is connected to the DC link capacitor which has a large capacitance to be able to store energy between each switching cycle as well as to filter out any voltage ripple in rectifier mode. The AC side of the converter is connected to the three phase grid through an inductance filter.

The filter is used to filter out any ripple in the incoming and outgoing current. The inductance of the filter is Lg and the equivalent resistance of the filter is small enough to be negligible so it is not shown in figure 1. Lg is set to a value of 0.5mH, which is large enough to filter out any current ripple. If necessary, the value of Lg as well as the converter switching frequency can be increased in order to meet the requirement of grid-side current THD of less than 5%.

The DC link capacitor is the interface between the dual active bridge and the full bridge converter. In figure 1, the dual active bridge and the battery are represented by a voltage source and a resistor in series - Edc and Rdc. Edc represents the voltage being contributed by dual active bridge and battery to the grid in inverter mode and the voltage being drawn by the battery and dual active bridge in rectifier mode. Rdc represents the equivalent resistance of the dual active bridge and battery. The voltage difference between Edc and Vdc - the DC link capacitor voltage - is what controls the direction of power flow for the full bridge converter.

Vdc can be calculated using the following formula [1]:

$$V_{dc} = \sqrt{6} V_g / m_a \quad \text{for } 0 < m_a \leq 1$$

where V_g is the rms value of the grid phase voltage and m_a is the modulation index. This sets the range for Vdc as $\infty < V_{dc} \leq 594V$.

When Edc<Vdc, Idc >0 and power flows from the grid the converter acts in rectifier mode [1]. When Edc>Vdc, Idc<0 and power flows to the grid and the converter acts in inverter mode [1].

Voltage/Current Transformation Blocks

$$\begin{bmatrix} x_d \\ x_q \end{bmatrix} = \frac{2}{3} \begin{bmatrix} \cos\theta & \cos(\theta - 2\pi/3) & \cos(\theta - 4\pi/3) \\ -\sin\theta & -\sin(\theta - 2\pi/3) & -\sin(\theta - 4\pi/3) \end{bmatrix} \cdot \begin{bmatrix} x_a \\ x_b \\ x_c \end{bmatrix} \tag{2}$$

abc to dq transformation [1]

$$\begin{bmatrix} x_a \\ x_b \\ x_c \end{bmatrix} = \begin{bmatrix} \cos\theta & -\sin\theta \\ \cos(\theta - 2\pi/3) & -\sin(\theta - 2\pi/3) \\ \cos(\theta - 4\pi/3) & -\sin(\theta - 4\pi/3) \end{bmatrix} \cdot \begin{bmatrix} x_d \\ x_q \end{bmatrix}$$

dq to abc transformation [1]

The grid side currents and voltages are converted from the stationary abc frame to the rotating dq frame using the abc/dq transformers and a PLL for tracking the angle of the grid side quantities. Figure 3 shows how a three phase quantity in the abc frame can be converted to the dq frame. There are many advantages to using the dq frame for controller design. One advantage is that it simplifies the problems of controlling three sinusoidal signals - one for each phase - into an equivalent problem of controlling two DC signals [2]. This greatly simplifies the controller design and allows the use of PI controllers. Another advantage is that the dq frame allows control of the d-axis and q-axis quantities independently of each other [1].

After the signals in the dq frame are compensated by their PI controllers, they are converted back to the abc frame for use in the PWM scheme used for generating the switching signals for the converter. Figure 4 shows the conversion process for transforming signals in the dq frame to the abc frame.

Theta_g Detector Block

The PLL is to sync the output oscillator signal with a reference signal. PLLs reduce the phase errors between input and output frequencies. The Simulink implementation of the Theta_g detector includes an abc/αβ transformation, a cartesian to polar transformation and an unit delay block. The Theta_g block is used to track the angle of the grid side quantities for use in the abc/dq and dq/abc transformations. The PLL ensures that the quantities in the rotating reference frame rotate at the same angular velocity as the grid side quantities [2]. This allows the quantities in the rotating reference frame to appear relatively stationary so they can be treated as DC quantities, which greatly simplifies the controller design process.

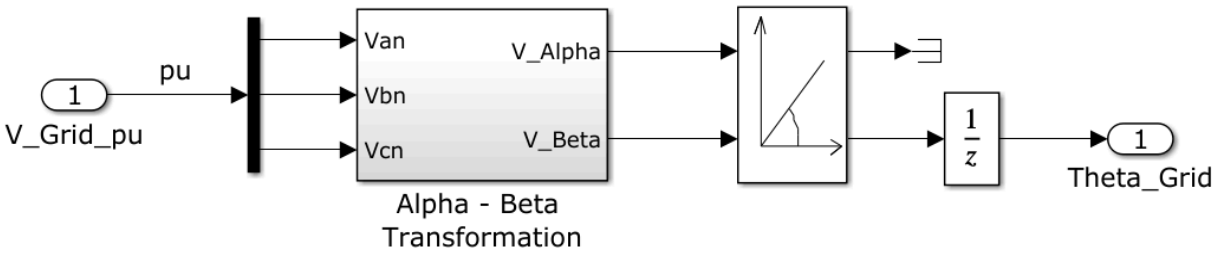

Figure 2.3: Simulink implementation of the Theta_g detector

PWM Block

The switching frequency is set to 10kHz to minimize the THD in the grid side current. If the THD needs to be further reduced, the switching frequency can be increased up to 20kHz. The inductance of the grid side filter can also be increased if needed to meet the requirement of grid side current THD of less than 5%. To generate the PWM signal, the signals output by the decoupled current controller, Vqi and Vdi, are passed through a dq/abc converter using theta_g to convert them to the abc frame. We needed to select “Aligned with phase A axis” under

parameters. This ensures that the dq0 components are d=0, and q= -π/2, which defines the alignment of the frames, meaning the d-axis is aligned with the phase A axis. These sinusoidal message signals are then compared with a triangle carrier wave that oscillates at the switching frequency of 10kHz. The resultant pulse width modulated signals store the amplitude of the message signals in their pulse-widths. Each signal is also inverted once to generate the switching signal for the opposite switch in each branch of the IGBT converter. The result is a total of six switching signals, once for each switch of the IGBT converter.

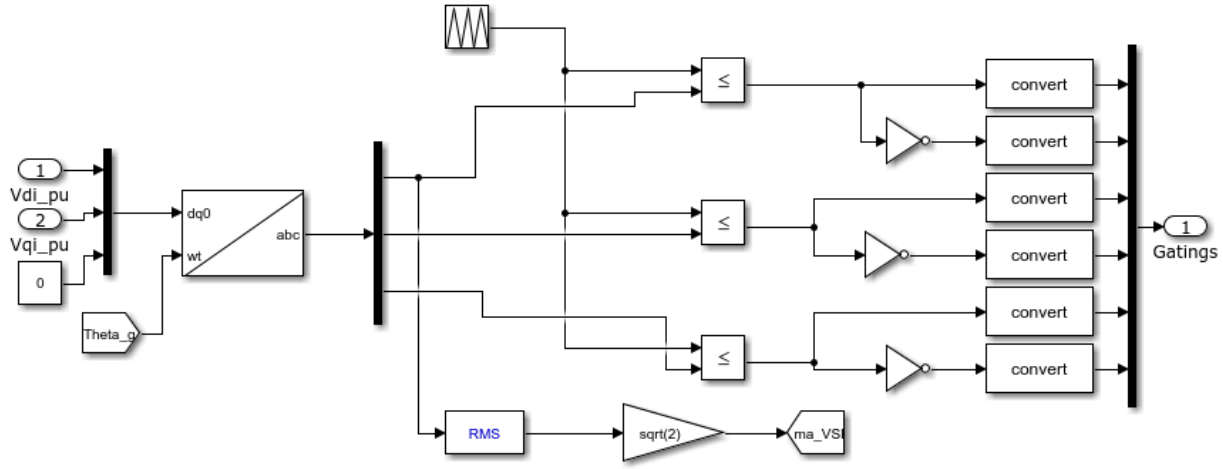

Figure 2.4: Simulink implementation of the PWM

Decoupled Current Controller

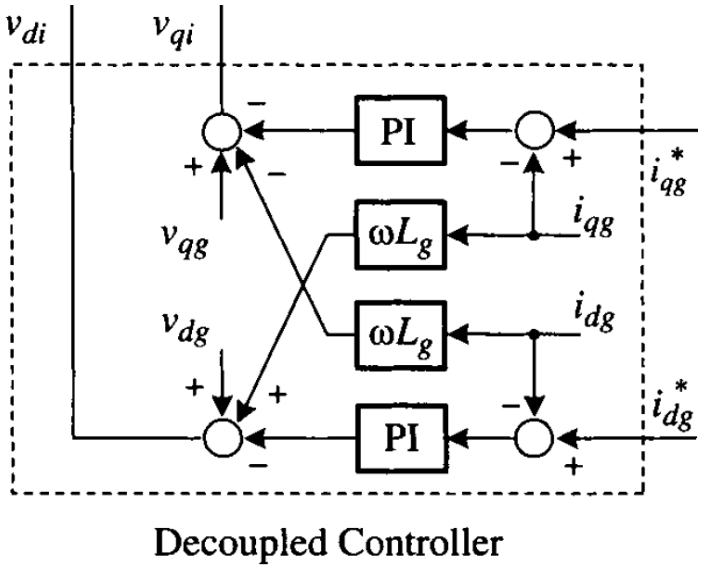

Figure 2.5: Decoupled current controller[1]

The goal of the current controller is to be able to independently control the d-axis and q-axis currents to be able to provide the input control signals for the PWM block. Input signals are the d-axis and q-axis voltages from the PLL as well as the reference current signals from the DC-link

controller. The d-axis and q-axis used the same values for the PI controller. Several methods were tried to tune the required PI controllers.

The closed loop response function is:

$$G_{CLi} = \frac{1+\frac{1}{K_{II}}\cdot s}{1+\frac{1}{K_{II}}\cdot s+\frac{L}{K_{II}\cdot K_{PI}}\cdot s^2} \tag{3}$$

Using the above equation, incorporating natural frequency and damping ratio, it is provided:

$$G_{CLi} = \frac{1+\frac{1}{K_{II}}\cdot s}{1+\frac{1}{K_{II}}\cdot s+\frac{L}{K_{II}\cdot K_{PI}}\cdot s^2} = \frac{1+\frac{2\cdot\zeta}{2\cdot\pi\cdot f_n}\cdot s}{1+\frac{2\cdot\zeta}{2\cdot\pi\cdot f_n}\cdot s+\left(\frac{1}{2\cdot\pi\cdot f_n}\right)^2\cdot s^2} \tag{4}$$

The PI controller parameters can then be found by using the provided equations:

$$K_{PI} = 4\cdot\pi\cdot BW_i\cdot L\cdot\zeta \tag{5}$$

$$K_{II} = \frac{2\cdot\pi\cdot BW_i}{\zeta} \tag{6}$$

We then use the following Percent overshoot and Tsettling equations to find the values for damping ratio and natural oscillation frequency.

$$\mathrm{PO} = 100\,e^{\frac{-\pi\zeta}{\sqrt{1-\zeta^2}}}\ (\%) \tag{7}$$

$$T_s(1\%) \cong \frac{4.6}{\zeta\,\omega_n} \tag{8}$$

The above equations on the Decoupled Current Controller are taken from "Voltage Oriented Control of a Three Phase Rectifier."[3]

The above method shows how the PI controllers can be tuned according to the required system response. Another method that was attempted was the use of the PID tuner function in the PID controller block inside MATLAB Simulink. Using frequency response based tuning, the tuner was tuned using trial and error to provide a phase margin of at least 45 degrees and a large bandwidth. The following transfer function was used to model the plant:

$$\frac{1}{Ls+(R+r_{on})}$$

Figure 2.6: Linearized model of the controller [2]

In this model, L is the filter inductance and R + r_{on} represents the filter resistance. This method resulted in a proportional gain of 0.34 and an integral gain of 204. These values can later be adjusted to fine-tune the response.

DC-link Voltage controller

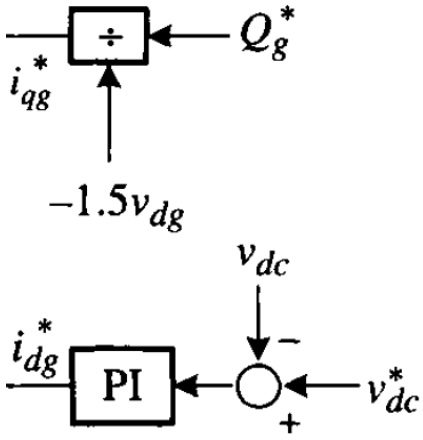

Figure 2.7: DC-link Voltage controller [1]

For this DC-link voltage controller, the goal is to maintain the DC bus voltage constant. This is done by comparing the DC voltage and the DC voltage reference. The resultant error signal is then passed to a PI controller. This project does not require the use of reactive power in either direction so Qg*, the reactive power reference, is set to 0.

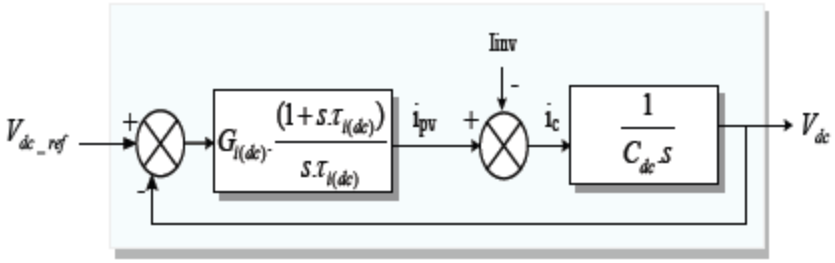

Figure 2.8: DC link voltage loop[3]

The closed loop transfer function is

$$FTBF_{dc}(s)=\frac{V_{dc}}{V_{dc\_ref}}=\frac{(1+s.\tau_{i(dc)})}{\frac{\tau_{i(dc)}.C_{dc}}{G_{i(dc)}}.s^2+\tau_{i(dc)}.s+1} \tag{9}$$

The PI controller parameters can then be found by using the provided equations:

$$G_{i(dc)}=2.\zeta_{(dc)}.C.\omega_{n(dc)}) \tag{10}$$

$$\tau_{i(dc)}=\frac{2.\zeta_{(dc)}}{\omega_{n(dc)}} \tag{11}$$

The above equations and diagrams on the DC-link Voltage controller are taken from "A Control Strategies of PV System based on VOC, SMC and MPC Algorithms"[4].

$$PO = 100\,e^{\frac{-\pi\zeta}{\sqrt{1-\zeta^2}}}\ (\%) \tag{12}$$

$$T_s(1\%) \cong \frac{4.6}{\zeta\omega_n} \tag{13}$$

Through the process of trial and error of using the overshoot percentage and Tsettling time as listed above, this method resulted in a proportional gain of 1 and an integral gain of around 200. These values may need to be changed or slightly tweaked later on.

3-1 DC-DC Converter

Dual Active Bridge Converter Circuit

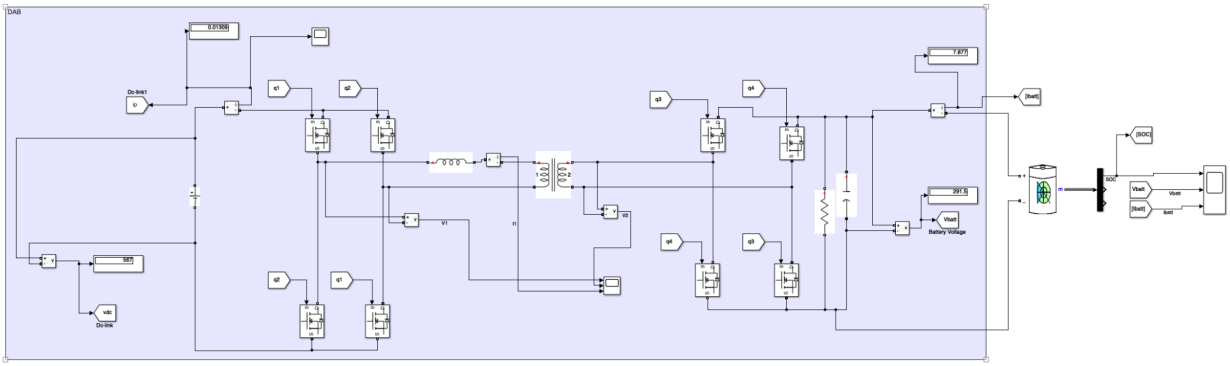

Figure 3.1: Dual active bridge design

The dual active bridge functions by turning a DC voltage source into a AC square wave voltage source via igbts. The igbts have a switching frequency to alternate from positive DC to negative DC thus making it a square wave. By turning the DC voltage into AC voltage, it enables us to use a transformer. Using the second bridge, it turns the AC voltage back into a DC voltage.
The dual active bridge above was designed using the following equations

$$P = \frac{Vin\,Vout\phi(1-\phi)}{\omega nL} \tag{14}$$

$$P = V_{out} I_{out} \tag{15}$$

$$V_{out} I_{out} = \frac{Vin\,Vout\phi(1-\phi)}{\omega nL} \tag{16}$$

$$I_{out} = \frac{Vin\,\phi(1-\phi)}{\omega nL} \tag{17}$$

This gives the output current. To get the output voltage,

$$V_{out} = \frac{Vin\,Vout\phi(1-\phi)}{I_{out}\omega nL} \tag{18}$$

It is also known that Vo/Io is equal to R. This leads to the above equation to be equal to

$$V_{out} = \frac{VinR\phi(1-\phi)}{2nLf} \quad (19)$$

Using the following equations, L can be calculated to meet the power output requirements. In the design, ω and R are variables that can be controlled.
Inductance and capacitance were found using the equation

$$L = Vin\phi(1 - \phi)n(Vout\ /2FPout) \quad (20)$$

$$c = Vin\phi^2 Ts^2((1 - \phi) + (\phi^2/4))/4nL \quad (21)$$

.

Using the variables that were established, it was found that the inductance value was $3.1687 \times 10^{-5} H$ and the capacitance value was $9.77 \times 10^{-3} F$.

Theoretically, the waveforms of the voltage before and after the transformer should be two square waves with a phase shift and a difference in magnitude. The current after the transformer should be a trapezoidal waveform.

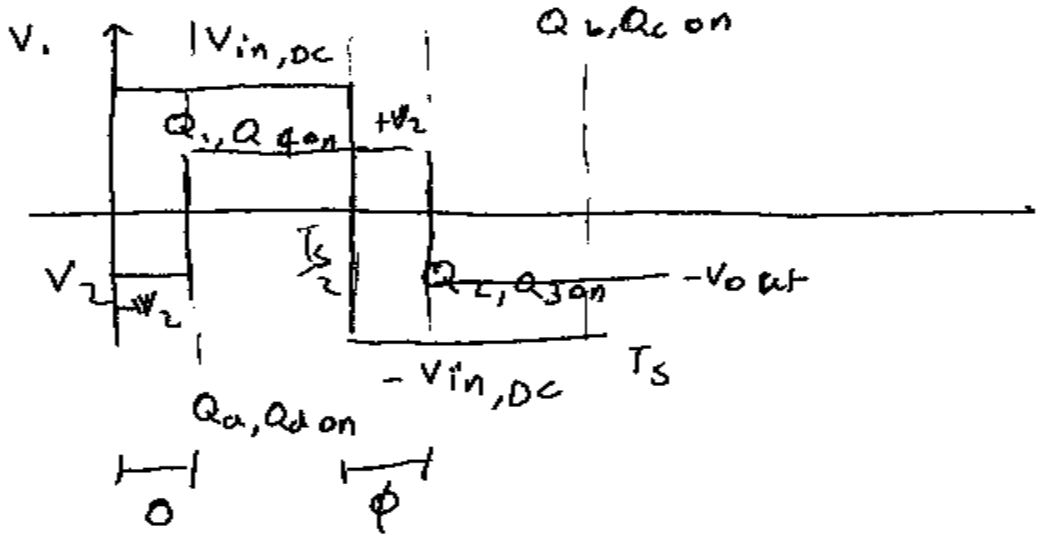

Figure 3.2: Intermediate voltage output

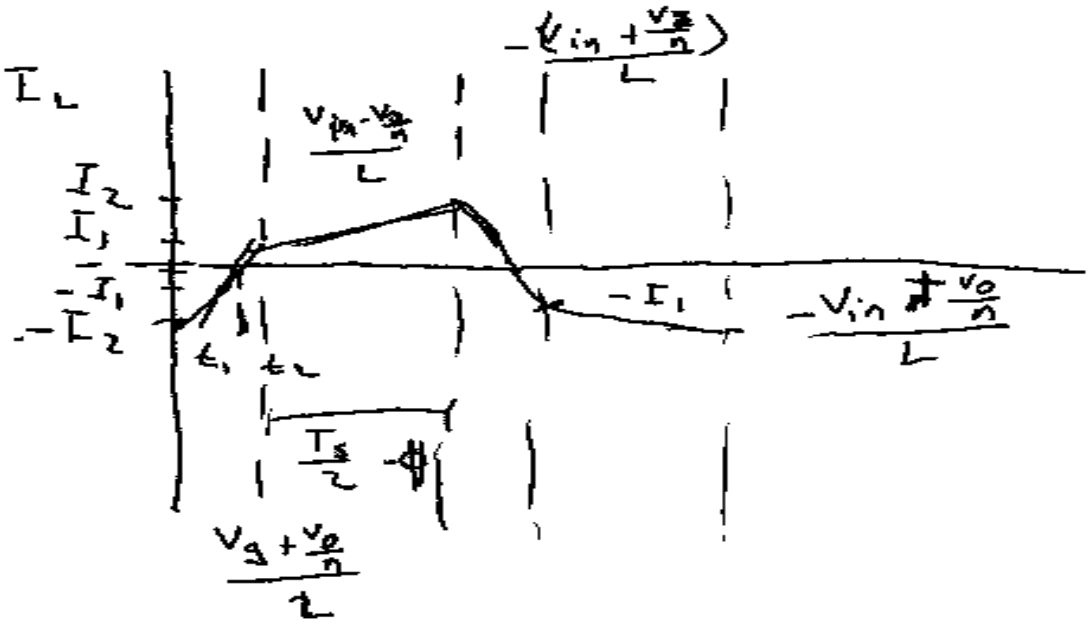

Figure 3.3: Intermediate current output

3-2 Dual Active Bridge Controller

To implement an accurate control of the Dual Active Bridge, a suitable switching scheme is required. The chosen components responsible are the IGBT MOSFET switches connected on either side of the transformer. These switches are turned on and off with oscillating signals with values of 0 and 1. To avoid unnecessary errors and to simplify the model two separate signals are generated, one consistent signal and the other with the imposed phase shift. Each signal and its inverse are fed to the switches on the appropriate side of the Dual Active Bridge.

For the system to operate as desired when charging, it must operate in two modes sequentially. These modes are Constant Current mode and Constant Voltage mode. When charging, the output of the DAB converter begins in Constant Current mode (CC). During this time, a constant output current is imposed as output voltage gradually rises. Once battery/output voltage has reached the desired value the system now operates in Constant Voltage mode (CV). From here on constant battery voltage is present as the State-Of-Charge continues to increase until full capacity is reached. This operation provides similar results when, alternatively, the battery is connected to a current source in place of the DAB or overall system. When discharging, the system is expected to run in Constant Power mode (CP). This mode operates quite like Constant Current mode, therefore, few changes are required during execution of such a control scheme.

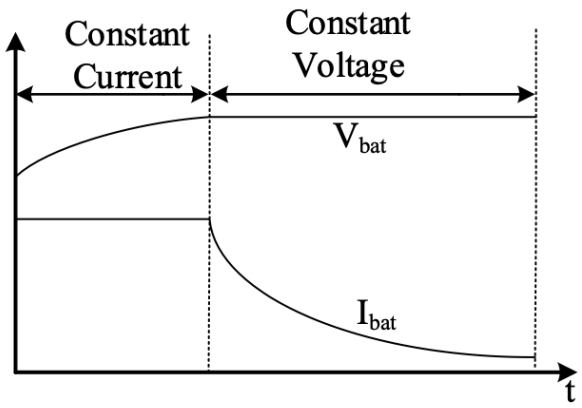

Figure 3.4: Relationship between the Battery Voltage and Current w.r.t time [5]

To effectively implement these modes the phase shift must be calculated as the system operates. The phase shift control is determined using a control scheme that takes into account the battery voltage and current at any given time. This system operates using a closed-loop control with the reference signal being the desired output voltage of the DAB converter. The error signal is passed through a PI controller and then used as the reference for the inner control loop responsible for the current control. The resultant signal from the overall closed-loop control provides a phase angle.

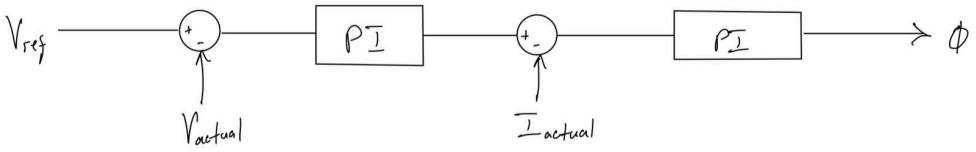

Figure 3.5: Dual active bridge design sketch

This phase angle must fall between the values of $\pm\pi/2$ radian. The sign of this angle results in the direction of power/current of the system, where positive values imply that the battery is charging and vice versa.

This chapter covered the design and theory of our models and parameters. Explanations and figures were shown to elevate the understanding of the V2G Electric Vehicle Quick Charger. The importance of specific blocks in the AC-DC converter were explained and how each block is used. The approach to find the parameters of the AC-DC converter were summarized above. The DC-DC converter is then explained in detail on the importance and use of the block. The obtaining of parameters were also discussed in terms of the DC-DC controller. The significance of each component was discussed and shown how it contributes to our final design. This section concludes our ideologies and theory regarding the V2G Electric Vehicle Quick Charger.

4 Alternative Designs

This section displays our alternative designs. Displayed are the attempted solutions to the V2G Electric Vehicle Quick Charger. A comparative analysis is included, showing what worked and what did not. Through this process, the final design can be concluded.

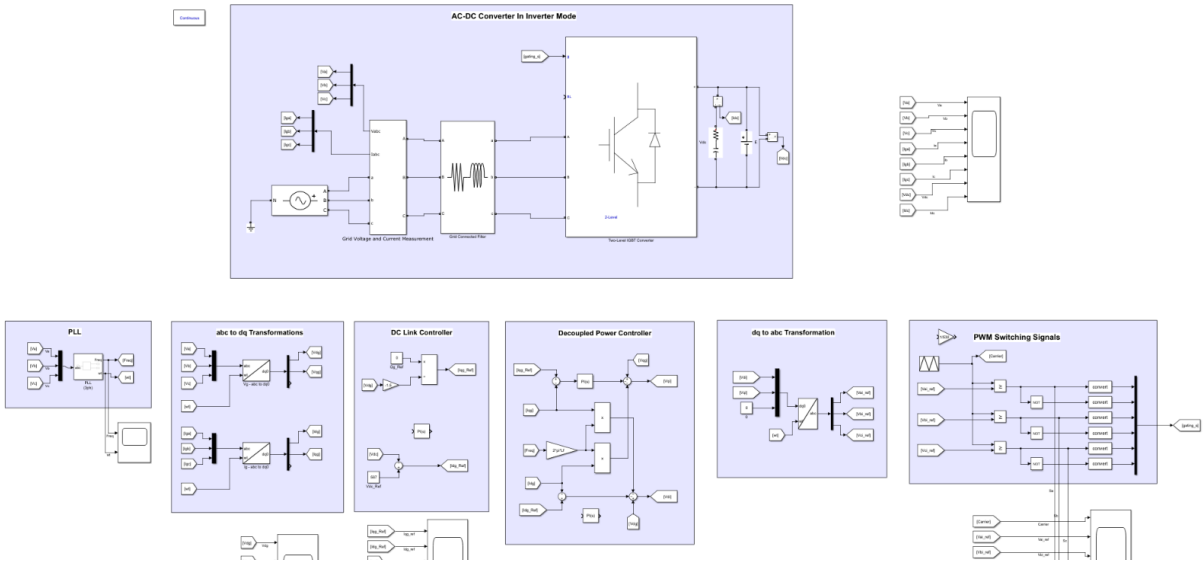

Figure 4.1: Initial model of the AC-DC converter and controller based on figure 2-1.

Figure 4-1 shows the first simulink model and its controller, with a design based on figure 2-1. This model was rejected due incorrect results caused by using actual values of current and voltage without being normalized or using the per unit system. The outputs based on actual values showed a very large gain in current and power waveforms. Due to this reason, the model in figure 5-1 was selected instead.

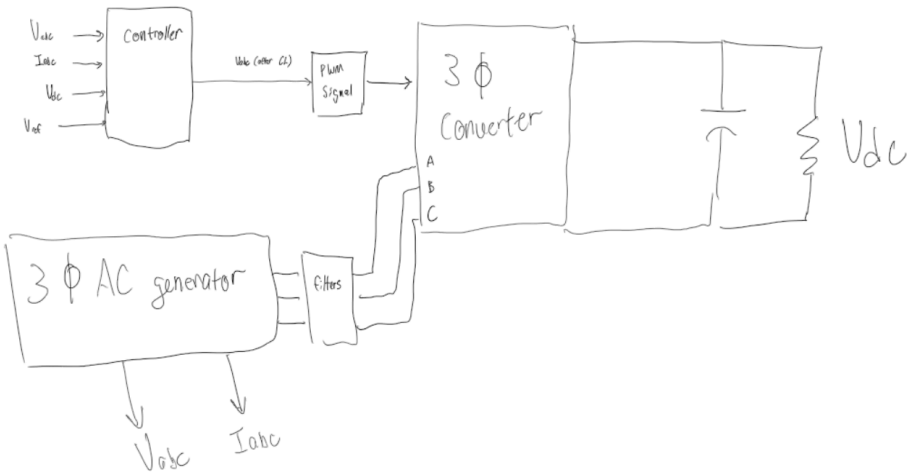

Figure 4.2: Initial design of AC-DC controller with theoretical placement in accordance to a early AC-DC converter model

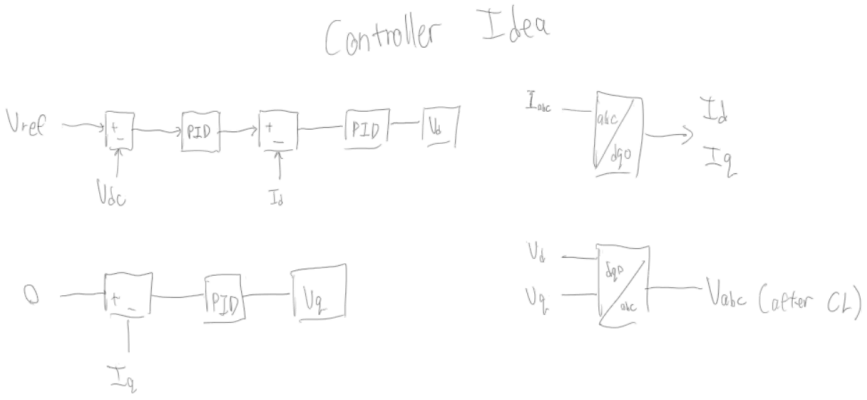

Figure 4.3: Initial design of AC-DC controller (Rectifier mode)

This early design was to be accompanied by the early stages of the AC-DC converter. Initially, the 2 modes of the AC-DC converter were separated, hence the use of controllers. The above model was planned for the rectifying mode of the converter. This design was referenced from a file from MathWorks File exchange. The model was modified inorder to fit the needs, but unfortunately it did not work well, due to the tuning process being trial and error, the results were not as expected. It was also quite difficult to tune the values, due to the lack of a abc/dq0 transformation. Due to this reason, the decoupled current controller and DC link controller was selected. This enabled easier tuning of parameters due to the ability to control the d and q axis separately.

An initial design for the Dual Active Bridge controller incorporated function blocks that took into account the power entering and leaving the DC-link capacitor.Assuming a fixed DC-link voltage (V_{DC}) at the end of the AC-DC converter, the voltage/current that charges the respective

capacitor at this junction should also leave within one switching cycle. As the incoming current (i_{ext}) changes, the DAB ensures V_{DC} remains constant with a phase shift.

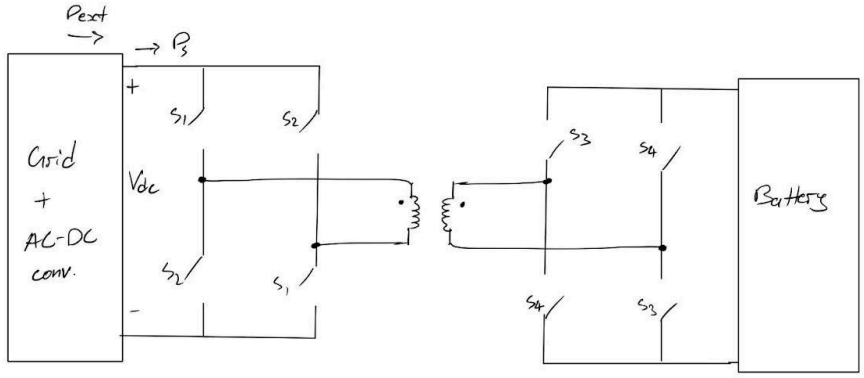

Figure 4.4: Initial design sketch of DAB model

Let $P_{ext} = i_{ext} \cdot V_{DC}$,

$dV_{DC}^2/dt = 2(P_{ext})/C - 2(P_S)/C + 2(Q_s)/C$; no reactance power expected

$= 2(P_{ext})/C - 2(P_S)/C$

From this analysis, the first stage of the control can be implemented. Using the expected V_{DC} and its actual value, a control scheme to determine the required output power from the capacitor is made. A tuned PI controller unit can be used here because of the use of DC values.

The equation for the expected output power with respect to the phase shift is:

$$P_{SO} = g \cdot \frac{V_{batt}^2}{\omega L} \cdot \phi(1 - \phi)$$

Where, V_{batt} is the battery voltage

g is the gain = V_{DC}/V_{batt}

ω is the switching frequency

If we rearrange the equation and solve for ϕ, we get

$$\phi = \frac{1}{2}\left(\pi \pm \sqrt{\pi^2 - \frac{4\pi\omega L P_{SO}}{g \cdot V_{batt}^2}}\right)$$

This value would return two roots. However, the relationship between P_{SO} and ϕ is positive between 0 and π, and negative between $-\pi$ and 0 with maximum power delivery at $|\pi/2|$ rad. The next stage of the controller is implemented using the equation above.

If one considers the sign of power from the AC-DC converter to the battery to be positive then the resultant phase shift will likewise be positive and vice versa. With the phase shift acquired from the combined stages this value is then fed into a function block to create two separate PWM signals which in turn are fed to the DAB.

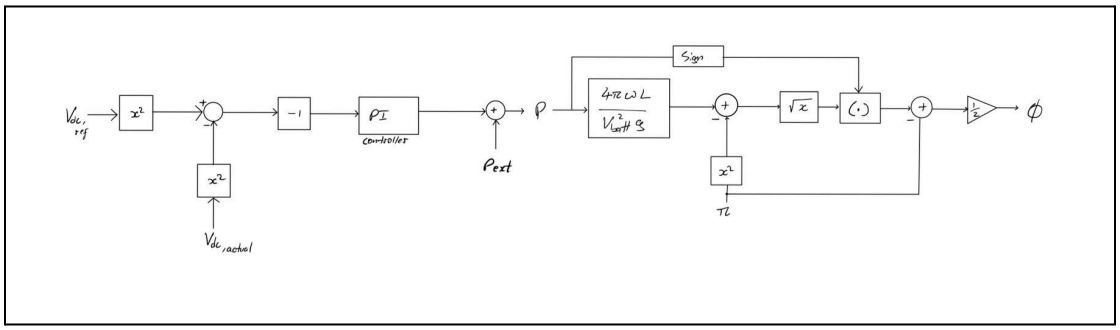

Figure 4.5: Initial design of DAB controller

This concludes the alternative design portion. Through multiple iterations, the final design was formed. This section showed the importance of troubleshooting and fixing the design. Using qualitatively or quantitatively comparisons allowed for the final design to flourish. Through these comparisons, allowed crucial decisions to be made.

5 Measurement and Testing Procedures

This section displays our measurements and testing procedures. Included below are the block diagrams of the AC-DC and its parameters, as well as the DAB. Simulation was performed using MATLAB Simulink and results were captured from the plots using the required testing conditions. Since the project consisted of two major components - the AC-DC converter and the DC-DC converter, they were first simulated separately and once successful, they could be combined into a single two-stage converter.

Below is the Simulink model and the parameters used for the AC-DC converter. The battery banks represent the DAB and the battery and were modeled using a DC voltage source; the three phase grid used the parameters listed in the requirements section.

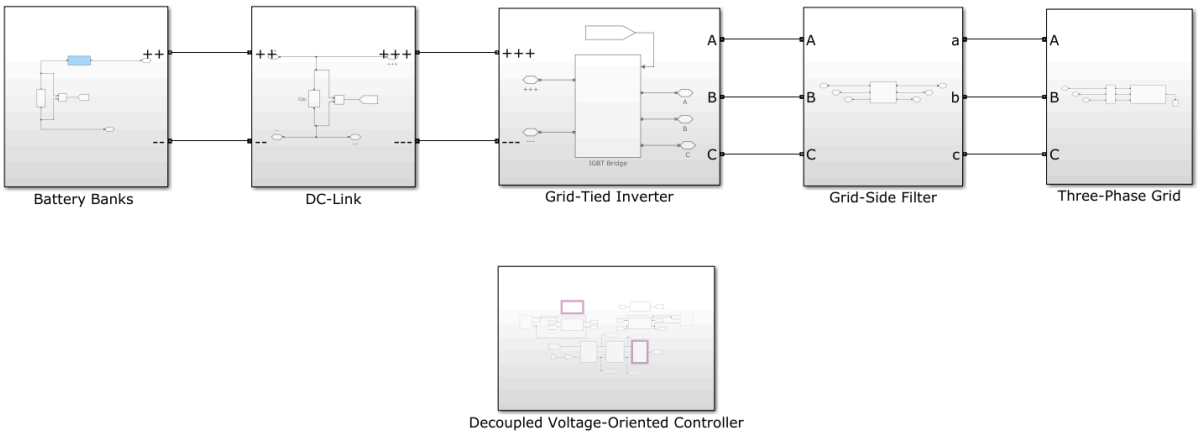

Figure 5-1: Simulink model of the AC-DC converter.

The figure below shows the simulink model used for testing and reworking the DAB converter model and its respective controller. To the left of the image is a DC voltage source representing the output from the AC-DC converter and the DC-link capacitor between the models. When testing, the scopes and windows shown aid in providing a clear understanding of which components or sets of components are functioning as desired.

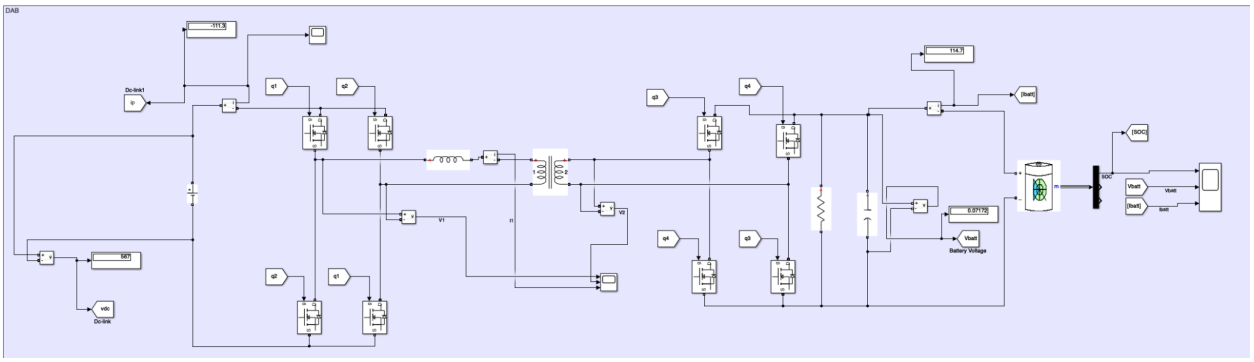

Figure 5-2: Simulink model of the DAB converter.

This concludes the Measurement and Testing Procedures section. Simulating the two major components: AD-DC converter and the DAB was done through MATLAB Simulink. Using the parameters provided above, the simulations were acquired and shown in the next section. After the confirmation of both working models, the two major components would be then connected through Simulink.

6 Performance Measurement Results

This section displays the performance of the V2G Electric Vehicle Quick Charger. Through MATLAB, the simulation results are provided below. First, the AC-DC converter results are shown below. The results include THD<5% and the converter working in both rectifying and inverting mode. Next the results of the DAB are shown. DAB's intermediate results are shown below.

AC-DC Converter Simulation Results

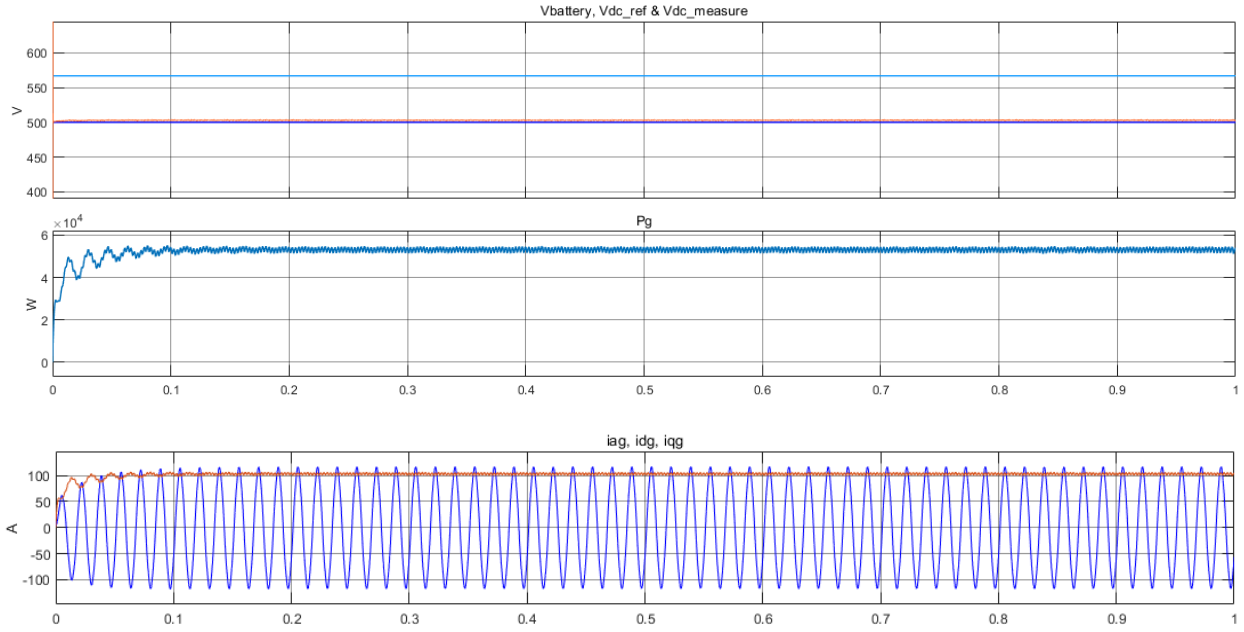

Figure 6-1: Rectifier mode results showing that with E<Vdc, Idc>0 and Pg>0.

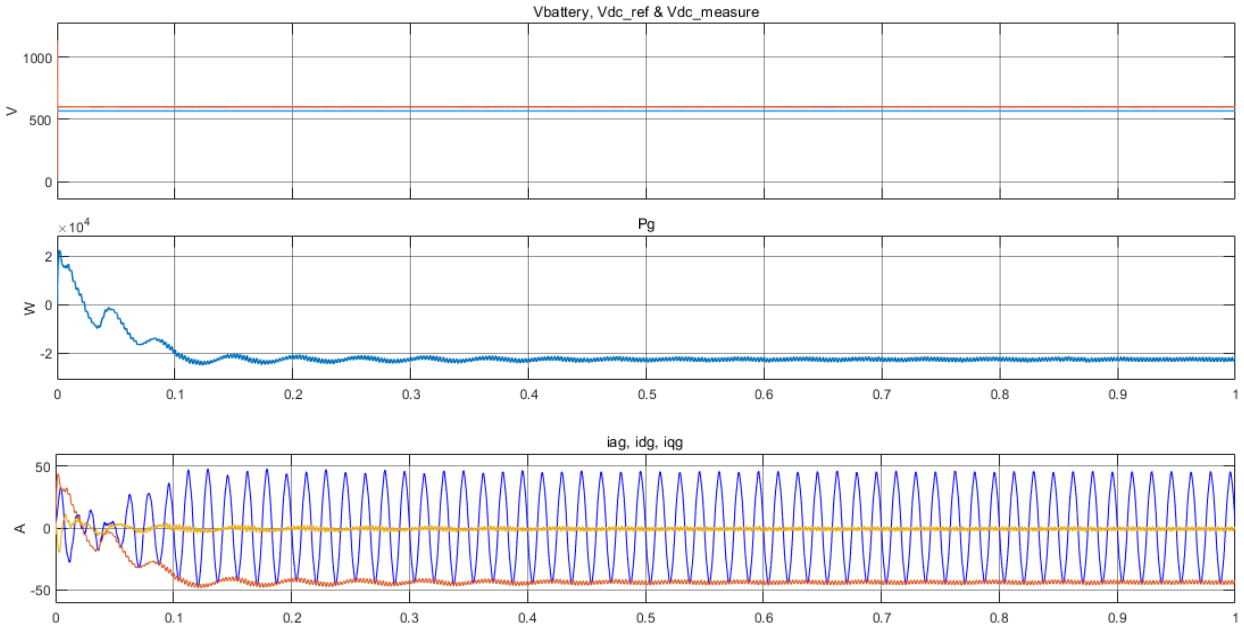

Figure 6-2: Inverter mode results showing that with E>Vdc, Idc<0 and Pg<0.

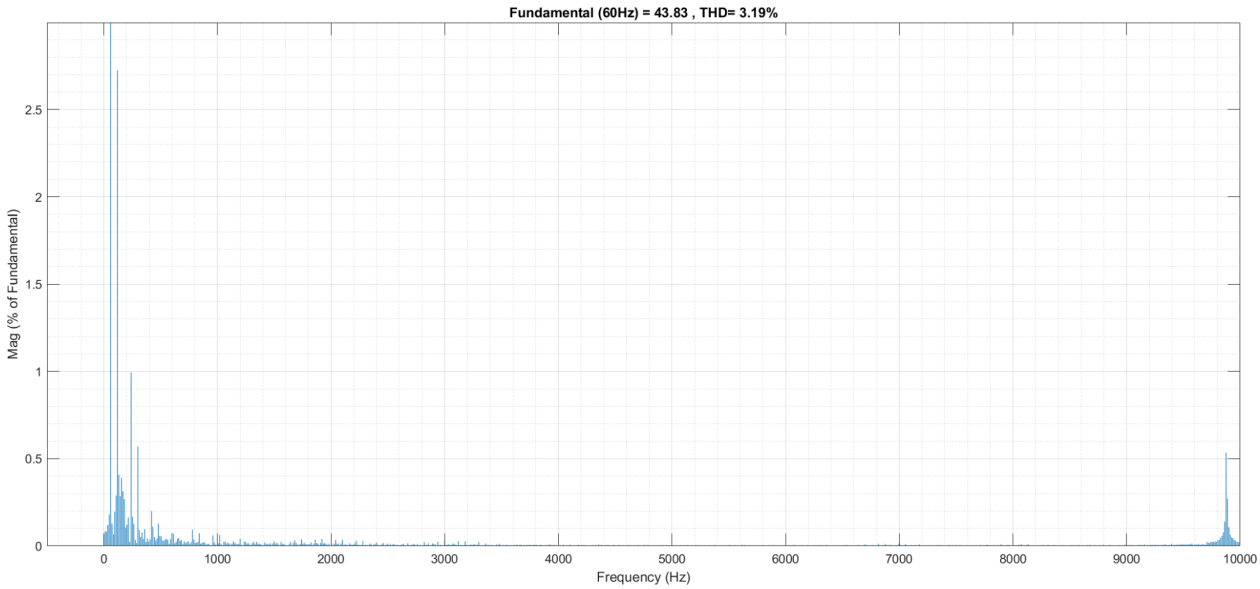

Figure 6-3: FFT analysis of the inverter current showing THD=3.19%.

Dual Active bridge simulation results

The following figure shows the voltage and current waveform before and after the transformer. The blue square waveform is the voltage after the transformer and the orange square waveform is the voltage before the transformer. The orange trapezoidal waveform is the current.

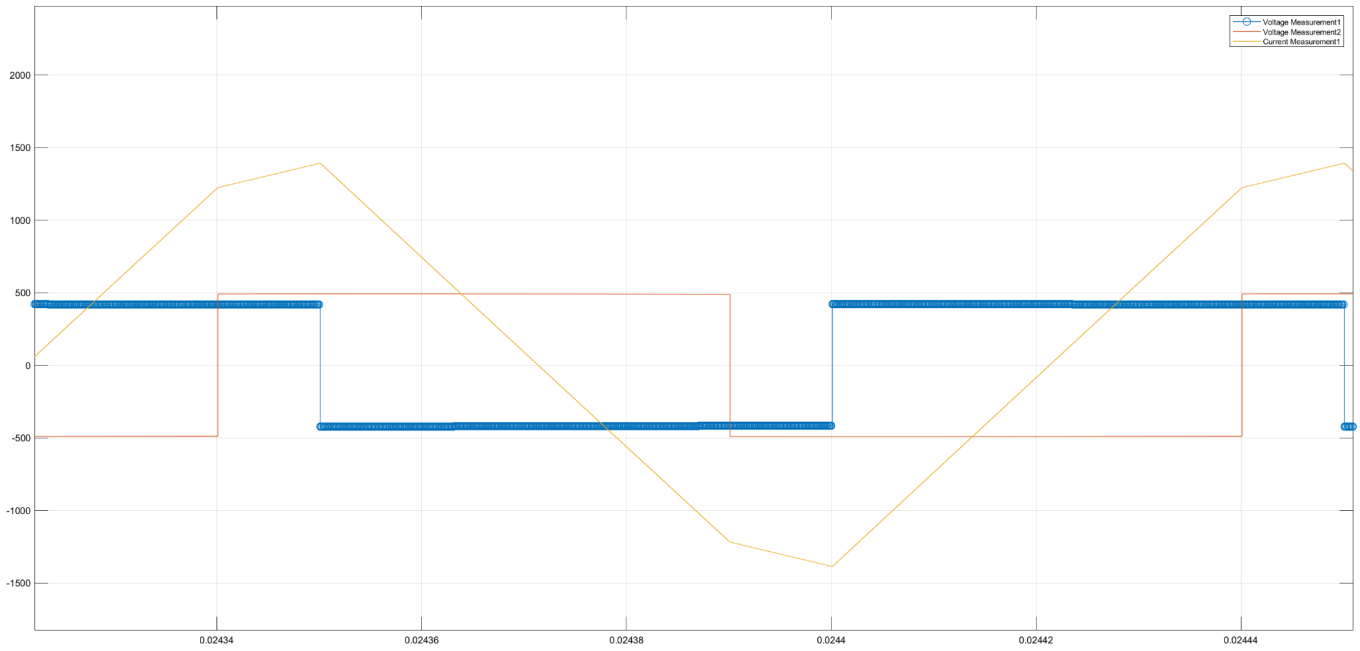

Figure 6-4: Dual active bridge intermediate results

The figure below represents the output of the localized Dual Active Bridge as it approaches Constant Voltage mode. The top graph represents the State-of-Charge of the battery and the bottom graph represents the output/battery voltage.

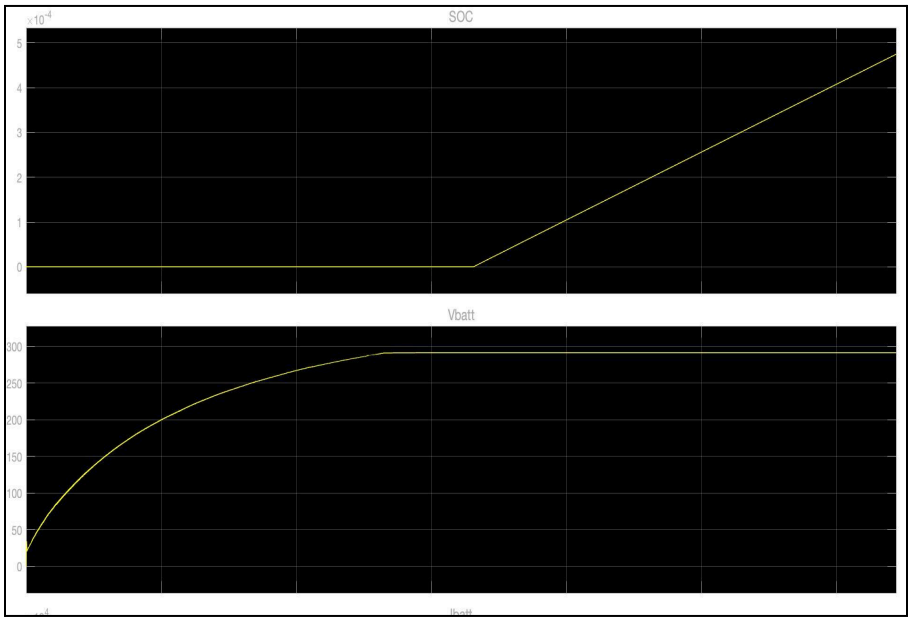

Figure 6-5: Localized Dual Active Bridge output

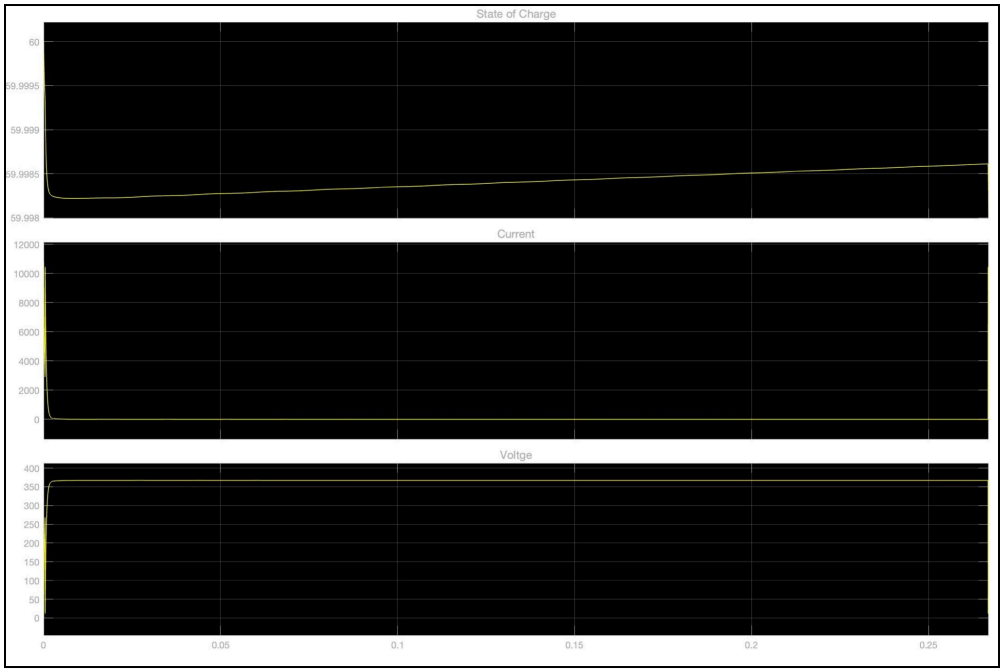

Figure 6-6: Output from Dual Active Bridge in connected system

This concludes the Performance Measurement Results section. The results of the AC-DC converter can be summarized through Figures 6-1 to 6-3. These figures display the converter working in both modes, and the ability to have bi-directional power flow. The simulation results of the DAB are shown to prove to be a working model.

7 Analysis of Performance

This section details the analysis of the simulation results in Chapter 6: performance measurements. The simulation results are compared with the project requirements and analyzed to determine if the requirements were satisfied. In the case they were not satisfied, possible explanations are provided. Since the converters were tested separately, the results of each converter are analyzed separately and compared against the requirements that were to be met by the respective converter.

AC-DC Converter Analysis

The ACDC converter was able to demonstrate bidirectional power flow as required. The flow of power in the single stage converter can be controlled with the voltage difference between the battery banks and the DC link voltage. Since the battery banks represent the DAB and the EV battery, the flow of power in the two stage converter can be controlled using the DAB when combined. The converter was also able to demonstrate contributing power to the grid at the grid frequency of 60hz and the grid voltage of 420V RMS. In inverter mode, the grid side current THD was also demonstrated to be less than 5% as required. However, the grid side inductance filter of the ACDC converter caused some issues with the total power of the system. The rated power had to be set lower than the required value of 60KW due to using an inductance that was too low. This may be due to the fact that the filter values were selected based on a typical range rather than calculated. In the future, the inductance of the filter should be more carefully calculated to provide a low THD as required but allow for the required power rating.

Dual Active Bridge Converter Analysis

From figure 6-4, it can be seen that the voltage and current waveforms follow the theoretically waveform. For testing purposes, the controller was not used and the phase shift was set to an arbitrary value. The reason the current reaches as high as it does is because the phase shift was significantly greater than the maximum value that the controller could provide.

The figure 6-5 shows one the latest results from the DAB model. From these values, it is clear that the functionality of the system has been partially met as constant voltage operation has been achieved while charging occurs. These results show that both the Dual Active Bridge and its respective controller do function nearly as intended. The output voltage falls within the range specified within the Objectives and state of charge increases at an appeasing rate. However, the current produced (Figure 6-6) does fall within preferred parameters and as a result prevents the full realization of the system.

This chapter provided an analysis of the simulation results from the previous chapter. The results were compared with the project requirements to determine if the requirements were met. In the case they were not met, a possible explanation was provided. Each stage was analyzed separately to determine if it met its respective requirements. The ACDC converter met all requirements except for the power rating. The dual active bridge was able to achieve constant voltage charging but not constant current charging.

8 Conclusions

This section summarizes what has been completed. Any discrepancy between the initial project objectives are to be found in this section. Included are major difficulties encountered that have not been resolved. Lastly any future work will be covered in this section.

To meet the objective of designing and simulating a two-stage bidirectional V2G electric vehicle charger, this project tested the two stages separately, with the goal of combining the two stages once each stage had been completed. Each stage made significant progress towards completion but due to the difficulties encountered along the way, the stages could not be completed on time and the two-stage converter could not be finished.

The ACDC converter met the requirements of bidirectional power flow, three phase grid interface, and the current THD of less than 5%. However, due to a poor choice of parameters, the rated power requirement could not be met. In the future, the inductance of the filter should be more carefully calculated to provide a low THD as required but allow for the required power rating.

The dual active bridge met the requirement of bidirectional power flow and constant voltage control. The requirements on constant current control and constant power control however were not met. The reason this is the case is unknown, and would require more time to resolve.

9 References

[1] B. Wu, *Power conversion and control of Wind Energy Systems*. Piscataway, NJ: IEEE Press, 2011.

[2] Y. Amirnaser, *Voltage - sourced converters in power systems: Modeling, control, and applications.* New Jersey: IEEE Press, 2012.

[3] J. Garcia, “Voltage oriented control of a three phase rectifier.,” *Lemuruniovi*. [Online]. Available:https://lemuruniovi.com/wp-content/uploads/2021/03/Voltage-Oriented-Control-of-a-Three-Phase-Rectifier.pdf. [Accessed: 14-Feb-2022].

[4] H. Laabidi, H. Jouini, and A. Mami, “A control strategies of PV system based on VOC, SMC and MPC algorithms,” *SRS Journal*, 21-Aug-2019. [Online]. Available: https://indjst.org/articles/a-control-strategies-of-pv-system-based-on-voc-smc-and-mpc-algorithms. [Accessed: 14-Feb-2022].

[5] Bao, Li, Lingling Fan, and Zhixin Miao, "Real-Time Simulation of Level 1, Level 2, and Level 3 Electric Vehicle Charging Systems," [Online]. Available: https://arxiv.org/abs/2111.02506. [Accessed: 01-Mar-2022]

[6] D. D. M. Cardozo, J. C. Balda, D. Trowler and H. A. Mantooth, "Novel nonlinear control of Dual Active Bridge using simplified converter model," *2010 Twenty-Fifth Annual IEEE Applied Power Electronics Conference and Exposition (APEC)*, 2010, pp. 321-327, doi: 10.1109/APEC.2010.5433651.

[7]T. Canada, “Minister of transport announces the expansion of the incentives for Zero-emission vehicles program,” *Canada.ca*, 22-Apr-2022. [Online]. Available: https://www.canada.ca/en/transport-canada/news/2022/04/minister-of-transport-announces-the-expansion-of-the-incentives-for-zero-emission-vehicles-program.html. [Accessed: 01-May-2022].

10 Appendices

```
% Grid Parameters
Vg = 420;                       % Grid Line-Line rms Voltage (V)
Fg = 60;                        % Grid Frequency (Hz)
Sg = 15e3;                       % Rated Power of the Grid (VA)

% Grid Base Values and pu Calculations
Sbg = Sg/3;                     % Base Apparent Power (VA)
Fbg = Fg;                       % Base Frequency (Hz)
wbg = 2*pi*Fbg;                 % Base Electrical Frequency (rad/sec)
Vbg = Vg/sqrt(3);               % Base Voltage (V)
Ibg = Sbg/Vbg;                  % Base Current (I)
Zbg = Vbg/Ibg;                  % Base Impedance (ohm)
Lbg = Zbg/wbg;                  % Base Inductance (H)
Cbg = 1/(Zbg*wbg);              % Base Capacitance (F)

% Grid-side Filter Parameters Calculation
Rgf_pu = 0.005;                 % Grid Filter Leakage Resistance (pu) (not a physical element)
Lgf_pu = 0.2;                   % Grid Filter Inductance (pu)
Rgf = Rgf_pu*Zbg;               % Grid Filter Resistance (ohm)
Lgf = Lgf_pu*Lbg;               % Grid Filter Inductance (H)

% Peak Base Values Calculation for Control and Measurements
Vbgp = Vbg*sqrt(2);             % Peak Base Voltage (V)
Ibgp = Ibg*sqrt(2);             % Peak Base Current (I)

R_dc = 0.03;                    % DC-Link resistor value#2 (ohm) for 0.8 pu output power
C_dc = 4*Cbg;                   % DC-Link capacitor value (F) - 4.0 pu
```

Figure 10-1: MATLAB code for initialization of AC-DC converter parameters.